

Vertical displacement oscillatory modes in tokamak plasmas

*Original*

Vertical displacement oscillatory modes in tokamak plasmas / Barberis, T.; Yolbarsop, A.; Porcelli, F.. - In: JOURNAL OF PLASMA PHYSICS. - ISSN 0022-3778. - ELETTRONICO. - 88:5(2022). [10.1017/S0022377822000988]

*Availability:*

This version is available at: 11583/2972550 since: 2022-10-24T08:28:34Z

*Publisher:*

Cambridge University Press

*Published*

DOI:10.1017/S0022377822000988

*Terms of use:*

This article is made available under terms and conditions as specified in the corresponding bibliographic description in the repository

*Publisher copyright*

(Article begins on next page)

# Vertical displacement oscillatory modes in tokamak plasmas

T. Barberis<sup>1</sup>, A. Yolbarsop<sup>1,2</sup> and F. Porcelli<sup>1,†</sup>

<sup>1</sup>Department of Applied Science and Technology, Polytechnic University of Turin, Torino 10129, Italy

<sup>2</sup>KTX Laboratory and Department of Engineering and Applied Physics, University of Science and Technology of China, Hefei, Anhui 230022, PR China

(Received 7 June 2022; revised 20 September 2022; accepted 21 September 2022)

Vertical displacement normal modes in shaped tokamak plasmas are studied analytically, based on the reduced ideal-magnetohydrodynamic model. With the help of quadratic forms, and using the appropriate eigenfunction for vertical displacements with toroidal mode number  $n = 0$  and dominant elliptical-angle mode number  $m = 1$ , a dispersion relation is derived, including the effects of ideal or resistive walls through a single parameter,  $D_w(\gamma)$ , which is, in general, a function of the complex eigenfrequency  $\gamma = -i\omega$ . For the resistive-wall case, the dispersion relation is cubic in  $\gamma$ . One root corresponds to the well-known, non-rotating resistive-wall vertical mode, growing on the resistive-wall time scale. The other two roots are weakly damped by wall resistivity, but oscillate with a frequency below the poloidal Alfvén frequency, which makes them immune to continuum damping, but subject to possible instability due to resonant interaction with fast ions.

**Key words:** fusion plasma, plasma instabilities, plasma waves

## 1. Introduction

Tokamak plasma discharges with non-circular cross-section are common features in modern-day magnetic fusion experiments. An important advantage of such configurations is higher instability thresholds, in terms of toroidal plasma current and beta (=kinetic/magnetic pressure) values, against ideal-magnetohydrodynamic (MHD) modes. Furthermore, plasma shaping is associated with magnetic divertors, which ameliorate the problem of plasma-wall interaction and allow access to high confinement regimes (so-called H-modes, Wagner *et al.* 1982). On the other hand, elongated plasmas are prone to an instability, initiated by an axisymmetric perturbation with toroidal mode number  $n = 0$ , leading to vertical displacement events (VDEs) (Strait *et al.* 1991; Granetz *et al.* 1996; Albanese, Mattei & Villone 2004; Riccardo & JET EFDA Contributors 2009), where the entire plasma shifts vertically until it touches the vacuum chamber. Uncontrolled VDEs must be avoided, as they lead to plasma current disruptions, which are dangerous in that they can severely damage the first wall of the vacuum chamber and the mechanical

† Email address for correspondence: [francesco.porcelli@polito.it](mailto:francesco.porcelli@polito.it)

structure of the tokamak device. For this reason, a vast amount of literature has been dedicated to the theoretical study of vertical plasma displacements, starting from the pioneering work by Laval, Pellat & Soule (1974), and continuing throughout the years (Okabayashi & Sheffield 1974; Haas 1975; Rebhan 1975; Perrone & Wesson 1981; Lazarus, Lister & Neilson 1990; Fitzpatrick 2009; Zakharov, Galkin & Gerasimov 2012; Portone 2017; Clauser, Jardin & Ferraro 2019; Krebs *et al.* 2020 provide a non-exhaustive sample), up until very recently, where the impact of magnetic divertor X-points on  $n = 0$  modes was analysed within the framework of the ideal-MHD model (Yolbarsop, Porcelli & Fitzpatrick 2021; Yolbarsop *et al.* 2022).

The focus of this article is, however, somewhat different. We derive analytically the dispersion relation for vertical displacement normal modes, and focus our attention on the oscillatory solutions, with a discrete frequency of oscillation in the poloidal Alfvén frequency range. These discrete modes, which we will refer to as ‘vertical displacement oscillatory modes’ (VDOM), are different from the well-known global Alfvén eigenmodes (Villard & Vaclavik 1997) with toroidal mode number  $n = 0$ , as discussed more at length in the Conclusion section. The VDOM are weakly damped by wall resistivity. The existence of these lightly damped solutions was noted before, see, e.g. Olofsson (2022) and Pfefferlé & Bhattacharjee (2018); however, in those references, the emphasis was on the growth and control of the usual, non-rotating vertical resistive wall mode, while the importance of the oscillatory solutions was played down. In fact, in our view, the VDOM solutions of the relevant dispersion relation are very interesting, as their oscillatory character opens the possibility that they are driven unstable by the resonant interaction with energetic particles, see also Barberis, Porcelli & Yolbarsop (2022). Observations of saturated  $n = 0$  oscillations were reported in recent JET experiments where energetic fast ion populations were produced by intense auxiliary plasma heating (Oliver *et al.* 2017; Kiptily *et al.* 2021).

Thus, this article contains two main results. The first result is a fully analytic derivation, based on the reduced MHD model, of the cubic dispersion relation for  $n = 0$  vertical modes with elliptical-angle mode number  $m = 1$ , valid for arbitrary values of the ellipticity parameter  $e_0$  (defined in (2.2) below), in the presence of a resistive wall. As far as we are aware, our analytic derivation is new and adds valuable insight into the frequency and spatial structure of the relevant  $n = 0$  modes. Analytic progress was possible thanks to the choice of a much idealized equilibrium, but we do hope that our analytic theory will motivate numerical work using more realistic tokamak geometries. The second result is a detailed discussion of the  $n = 0$  VDOM.

Our analysis adopts the same equilibrium configuration as Laval *et al.* (1974), where the plasma boundary and the nearby wall of the containment vacuum chamber are assumed to be confocal ellipses. Based on the ideal-MHD energy principle, it was concluded in Laval *et al.* (1974) that a perfectly conducting, ideal wall is capable of passively stabilizing vertical plasma displacements. Adding to the work of Laval *et al.* (1974) and of subsequent publications, our article presents the analytic derivation of the mode structure and cubic dispersion relation for vertical modes with toroidal mode number  $n = 0$  and elliptical-angle mode number  $m = 1$ . This dispersion relation is valid for arbitrary values of the ellipticity parameter; it includes the effects of a resistive wall through a single, frequency-dependent parameter,  $D_w(\gamma)$ , defined in (4.29) below. An in-depth discussion of the three relevant roots of the dispersion relation is presented. Under relevant experimental conditions, two of the three roots have a frequency of oscillation just below the poloidal Alfvén frequency and are weakly damped by wall resistivity. The third root, instead, is purely growing on the wall resistivity time scale; this third root is the usual, non-rotating

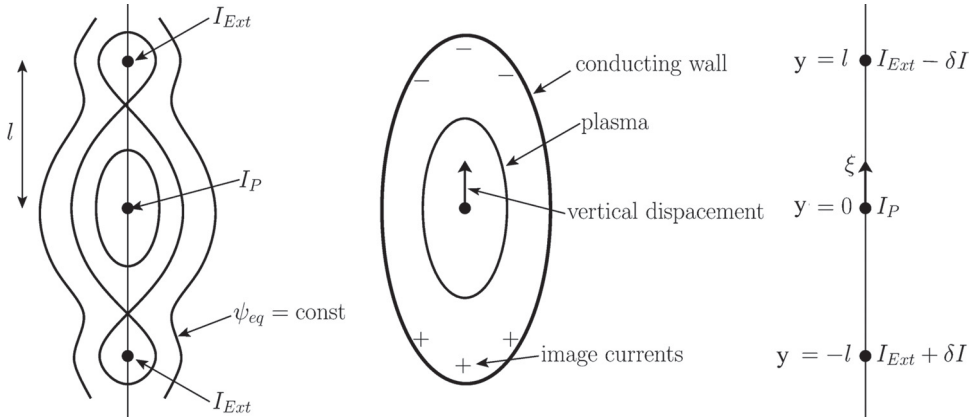


FIGURE 1. Schematic diagram of the heuristic model for the vertical instability.

vertical resistive-wall mode, which can be suppressed by active feedback stabilization (Lazarus *et al.* 1990; Lister *et al.* 1990; Albanese *et al.* 2004; Portone 2017).

This article is organized as follows. The cubic dispersion relation for  $n = 0$  modes is first derived heuristically in § 2. In § 3, the normal-mode spatial structure is resolved based on the reduced ideal-MHD model. The most original results are presented in § 4; in this section, first, a general dispersion relation is obtained with the use of quadratic forms; then, relevant solutions of the dispersion relation are obtained for three scenarios of interest: the no-wall case, the ideal wall limit and the case of a resistive wall. Conclusions are presented in § 5.

## 2. Heuristic model

Insight into the mechanism and time scales of the vertical instability can be gained with the help of a simple heuristic model, involving currents flowing in three parallel rectilinear wires. This toy model is well known, and a simple derivation of the relevant dispersion relation for the case of an ideal wall can be found, e.g. in Yolbarsop *et al.* (2021, 2022) and Pfefferlé & Bhattacharjee (2018). This calculation is repeated here for the reader’s convenience, together with its extension to the case of a resistive wall.

With reference to figure 1, let  $y$  be the vertical direction. The currents flow along the  $z$  direction, which mimics the toroidal direction of a tokamak plasma. The two ‘external’ currents,  $I_{Ext}$ , are equal and positive and are fixed at  $y = \pm l$ , while the ‘plasma’ current,  $I_p$ , can drift along the vertical direction. A vacuum surrounds the three wires. Clearly,  $y = 0$  is an unstable equilibrium point for the plasma wire. Also shown in figure 1 are magnetic X-points located at  $y = \pm l_y < l$ .

The equation of motion for the plasma wire is

$$\mu_m \ddot{y} = \frac{4 I_P I_{Ext}}{c^2} \frac{y}{l^2 - y^2}, \tag{2.1}$$

with  $\mu_m$  the linear mass density,  $c$  the speed of light and an over-dot denotes time derivative (c.g.s. units have been adopted). Neglecting self- and mutual induction currents,  $I_P$  and  $I_{Ext}$  remain constant as the plasma wire is displaced. For small  $y \ll l$ , the solution of (2.1) is  $y = y_0 e^{\gamma_H t}$ , where  $y_0$  is an initial displacement, and  $\gamma_H = (1/l)(4I_P I_{Ext}/\mu_m c^2)^{1/2}$ .

If, instead of a plasma wire, we consider a vertically elongated plasma with uniform current density up to an elliptical magnetic surface with minor semi-axis  $a$  and major

semi-axis  $b$ , then, according to the analysis of Porcelli & Yolbarsop (2019), a relationship is found involving the currents  $I_P$  and  $I_{\text{Ext}}$  and the distance  $l$ :  $I_{\text{Ext}}/I_P = [(b - a)/(b + a)] [l^2/(a^2 + b^2)]$ . With this expression,  $\gamma_H$  turns out to depend only on the plasma current  $I_P$  and on the semi-axes  $a$  and  $b$ , but not on  $I_{\text{Ext}}$  and  $l$ . Also,  $\mu_m$  can be replaced by  $\mu_m \rightarrow \pi a b \varrho_m$ , where  $\varrho_m$  is the volume mass density. After straightforward algebra, and taking the limit of small ellipticity,  $e_0 \ll 1$ , where

$$e_0 = \frac{b^2 - a^2}{b^2 + a^2}, \quad (2.2)$$

the growth rate can be written as

$$\gamma_H = e_0^{1/2} \tau_A^{-1}, \quad (2.3)$$

where  $\tau_A^{-1} = B_P'/(4\pi \varrho_m)^{1/2}$  is the inverse Alfvén time, and  $B_P'$  is the radial derivative of the poloidal magnetic field on the magnetic axis. Note that, for a circular plasma cross-section,  $e_0 = 0$  and the growth rate  $\gamma_H$  vanish. Considering typical values of present-day tokamak experiments,  $\gamma_H^{-1}$  is indeed a swift growth time of the order of a few microseconds.

A perfectly conducting wall close to the plasma can provide passive feedback stabilization of the vertical instability. The stabilization mechanism is explained as follows. When the plasma is displaced from its equilibrium position, image currents are induced at the wall. The sign of these currents is such that the corresponding net force opposes the motion of the plasma wire. In the heuristic model, we can model this effect by assuming two currents of opposite sign,  $\pm \delta I$ , proportional to the displacement of the plasma column, and localized at  $y = \pm l$ . Then,

$$L \delta \dot{I} = L D I_{\text{Ext}} \dot{y}/l, \quad (2.4)$$

where  $L$  is an effective inductance and  $D$  is a dimensionless proportionality constant, which, in the case of a tokamak plasma, can be determined in terms of the wall geometry (see § 4 here below). After straightforward algebra, and taking the limit  $y \ll l$ , the equation of motion modified by the feedback currents becomes

$$\mu_m c^2 \ddot{y} \approx 4 I_P I_{\text{Ext}} (1 - D) y/l^2. \quad (2.5)$$

Thus, the vertical instability is suppressed when  $D > 1$ , which, in the actual tokamak case, translates into a criterion related to the proximity of the wall to the plasma column. As we shall see in § 4, for the special case where the plasma boundary and the wall are modelled by confocal ellipses, the marginal stability criterion corresponds to the magnetic X-points lying on the wall, while feedback stabilization,  $D > 1$ , requires the X-points to lie beyond the wall. In the latter case, (2.5) implies that the plasma oscillates vertically with frequency

$$\omega = \pm \omega_H = \pm \sqrt{D - 1} \gamma_H. \quad (2.6)$$

These two solutions with frequency  $\omega = \pm \omega_H$  are a first indication of what we dub the VDOM.

For the more realistic case of a resistive wall, (2.4) is modified into

$$R\delta I + L\dot{\delta I} = LD I_{\text{Ext}}\dot{y}/l. \tag{2.7}$$

After straightforward algebra, and again in the limit  $y \ll l$ , we find

$$\mu_m c^2 \ddot{y} = 4I_p I_{\text{Ext}} \dot{y}/l^2 - 4I_p \delta I/l. \tag{2.8}$$

Eliminating  $\delta I$ , we obtain the third-order differential equation for  $y$

$$\ddot{y} + \frac{1}{\tau_R} \dot{y} + \omega_H^2 y - \frac{1}{\tau_R} \frac{\omega_H^2}{D-1} y = 0, \tag{2.9}$$

where  $\tau_R = L/R$  is the resistive-wall penetration time.

We restrict the discussion that follows to the limit  $D > 1$ . Thus, searching for solutions of the type  $y(t) \sim y_0 e^{\gamma t}$ , a cubic dispersion relation for complex  $\gamma$  is obtained

$$\gamma^3 + \frac{1}{\tau_R} \gamma^2 + \omega_H^2 \gamma - \frac{1}{\tau_R} \frac{\omega_H^2}{D-1} = 0, \tag{2.10}$$

where  $\omega_H$  is defined in (2.6). In the limit of small wall resistivity,  $\omega_H \tau_R \gg 1$ , the two VDOM oscillatory roots of the ideal wall case turn out to be damped; setting  $\gamma = -i\omega$ , the two damped modes have a complex frequency

$$\omega = \pm \omega_H - \frac{iD}{2(D-1)\tau_R}. \tag{2.11}$$

On the other hand, the third root corresponds to a purely growing resistive instability with a growth rate

$$\gamma = \frac{1}{(D-1)\tau_R} \equiv \gamma_R. \tag{2.12}$$

For this non-rotating, unstable mode, the inverse growth rate scales with  $\tau_R$ , which, for typical tokamak parameters, gives rise to a characteristic growth time of the order of a few milliseconds. It is then possible to counter the growth of the resistive-wall vertical instability by means of active feedback control associated with currents flowing outside the tokamak vacuum chamber (Lazarus *et al.* 1990; Lister *et al.* 1990; Albanese *et al.* 2004; Portone 2017). We point out that, as long as the VDOM are damped, and as long as their oscillation frequency is well separated from the bandwidth of the vertical stabilization closed loop, they are not expected to have an impact on the active feedback stabilization system applied to the non-rotating, vertical resistive-wall mode.

In § 4, a more general dispersion relation, valid for arbitrary values of  $e_0$ , is obtained based on a complete solution of the ideal-MHD normal-mode problem applied to  $n = 0$  perturbations. In the limit of small ellipticity, the general dispersion relation reduces to the cubic equation (2.10), confirming in this way the validity of the heuristic model.

### 3. Vertical rigid-shift mode structure

The analysis of this section follows that already published by us in Porcelli *et al.* (2021) and Yolbarsop *et al.* (2021, 2022), which we briefly summarize here for the reader's convenience. An adequate model for the normal-mode analysis of the vertical instability is the well-known reduced ideal-MHD model (Strauss 1976). For axisymmetric modes, toroidal effects do not play an important role and, therefore, the straight-tokamak

approximation is adopted. The magnetic field is  $\mathbf{B} = \mathbf{e}_z \times \nabla\psi + B_z \mathbf{e}_z$ , where  $\mathbf{e}_z$  is the unit vector along the ignorable  $z$ -direction, which mimics the toroidal coordinate, and  $B_z$  is constant. The plasma flow is  $\mathbf{v} = \mathbf{e}_z \times \nabla\varphi + v_z \mathbf{e}_z$ . In the standard low- $\beta$  limit for a tokamak plasma, the fields  $B_z$  and  $v_z$  decouple from the fields  $\psi$  and  $\varphi$ . Therefore, the magnetic flux function,  $\psi$ , and the streamfunction,  $\varphi$ , obey the model equations (Strauss 1976)

$$\frac{\partial\psi}{\partial t} + [\varphi, \psi] = 0, \tag{3.1}$$

$$\frac{\partial}{\partial t} \nabla \cdot (\varrho \nabla\varphi) + [\varrho, (\nabla\varphi)^2] + [\varphi, \varrho]U + [\varphi, U] = [\psi, J]. \tag{3.2}$$

In these equations, all quantities are dimensionless, brackets are defined as  $[\chi, \eta] = \mathbf{e}_z \cdot \nabla\chi \times \nabla\eta$ ,  $J = \nabla^2\psi$  is the normalized current density and  $U = \nabla^2\varphi$  is the normalized flow vorticity. Space and time are normalized as  $\hat{r} = r/r_0$ , where  $r_0 = ab/[(a^2 + b^2)/2]^{1/2}$  is a convenient equilibrium scale length, and  $\hat{t} = t/\tau_A$ , where  $\tau_A$  is the poloidal Alfvén time defined below (2.3). The dimensionless fields are normalized as  $\hat{\psi} = \psi/(B_p' r_0^2)$ ,  $\hat{\varphi} = (\tau_A/r_0^2)\varphi$ ; the plasma density is normalized to its on-axis value,  $\hat{\varrho} = \varrho_m/\varrho_{m0}$ , and the current density is  $\hat{J} = (4\pi/cB_p')J_z$ . In order to simplify the notation, over-hats are actually dropped in (3.1) and (3.2), and in the following.

At equilibrium, fields are stationary, and, by assumption, the equilibrium plasma velocity is negligibly small. The current density,  $J_{eq}$ , is assumed to be uniform up to an elliptical boundary with minor semi-axis  $a$  and major semi-axis  $b$ , and to drop to zero beyond that boundary, where vacuum is assumed. Clearly, the elliptical boundary must be a magnetic flux surface, which lies necessarily within the region bounded by the magnetic separatrix. In elliptical coordinates  $(\mu, \theta)$ , where  $x = A \sinh(\mu) \cos(\theta)$  and  $y = A \cosh(\mu) \sin(\theta)$ , with  $A = \sqrt{b^2 - a^2}$ , the elliptical boundary corresponds to  $\mu = \mu_b$ , such that  $a = A \sinh \mu_b$  and  $b = A \cosh \mu_b$ . The equilibrium current density is  $J_{eq}(\mu) = 2H(\mu_b - \mu)$ , where  $H(x)$  is the Heaviside unit step function.

According to the analysis of Porcelli & Yolbarsop (2019), in the plasma region inside the elliptical boundary, where  $\mu < \mu_b$  and  $\psi = \psi_{eq}^-$ , the solution of  $\nabla^2\psi_{eq}^- = 2$  that is well behaved on the magnetic axis and that reduces to a constant on the elliptical boundary is best written in terms of Cartesian components

$$\psi_{eq}^-(x, y) = \frac{1}{2} \left( \frac{x^2}{b^2} + \frac{y^2}{a^2} \right). \tag{3.3}$$

In the vacuum region outside the elliptical boundary, where  $\mu > \mu_b$ , the equilibrium flux  $\psi_{eq} = \psi_{eq}^+$  satisfies  $\nabla^2\psi_m^+ = 0$ . Here, and in the following, the superscripts ‘-’ and ‘+’ indicate the plasma and vacuum regions, respectively. As we assume no equilibrium current sheets,  $\psi_{eq}$  and its derivative along the normal to the boundary must be continuous across the boundary. The relevant analytic solution is

$$\psi_{eq}^+(\mu, \theta) = \frac{1}{2} + \alpha^2 \left\{ \mu - \mu_b + \frac{e_0}{2} \sinh [2(\mu - \mu_b)] \cos(2\theta) \right\} \tag{3.4}$$

with  $\alpha^2 = ab/r_0^2$  and  $e_0$  the ellipticity parameter defined in (2.2). Magnetic flux surfaces  $\psi_{eq}(\mu, \theta) = \text{const.}$  exhibit a magnetic separatrix at  $\psi_{eq}(\mu, \theta) = \psi_X = \mu_b \alpha^2$ , with X-points located at  $\mu = \mu_X = 2\mu_b$  and  $\theta = \theta_X = \pi/2 \pm n\pi$ .

The equilibrium plasma density profile is also assumed to be uniform up to the elliptical boundary  $\mu = \mu_b$ , i.e.  $\varrho_{eq} = H(\mu_b - \mu)$ . Thus, this model equilibrium, where the plasma

terminates well before the magnetic separatrix, and a wall is present, resembles more closely a limiter tokamak scenario, with the equilibrium magnetic X-points that may lie either outside the plasma containment chamber, or in the vacuum region inside the chamber.

Two main reasons justify the choice of this particular equilibrium. First, we intend to carry out a fully analytic treatment of the normal-mode problem, which can be done if the starting point is a relatively simple equilibrium. The second is that, based on previous studies of the vertical stability problem, effects associated with gradients of the equilibrium plasma current density are not expected to play an important role. Furthermore, the equilibrium adopted in this article is the same as that used in Laval *et al.* (1974). On the other hand, equilibrium flows are neglected in this article and ought to be considered in future studies.

For stability considerations, set  $\psi(\mu, \theta, t) = \psi_{\text{eq}}(\mu, \theta) + \tilde{\psi}(\mu, \theta) e^{\gamma t}$  and  $\varphi(\mu, \theta, t) = \tilde{\varphi}(\mu, \theta) e^{\gamma t}$ , where the over-tilde denotes small perturbed quantities and  $\gamma = -i\omega$ . The linearized versions of (3.1) and (3.2) are

$$\gamma \tilde{\psi} + [\tilde{\varphi}, \psi_{\text{eq}}] = 0, \tag{3.5}$$

$$\gamma \nabla \cdot (\varrho_{\text{eq}} \nabla \tilde{\varphi}) = [\tilde{\psi}, J_{\text{eq}}] + [\psi_{\text{eq}}, \tilde{J}]. \tag{3.6}$$

In the region  $\mu < \mu_b$ , the streamfunction corresponding to a rigid vertical shift is represented in elliptical coordinates by

$$\tilde{\varphi}(\mu, \theta) = \gamma \xi a \frac{\sinh \mu}{\sinh \mu_b} \cos \theta, \tag{3.7}$$

where  $\xi$  is the vertical displacement of the plasma column. From the flux freezing condition (3.5) we obtain the corresponding perturbed magnetic flux

$$\tilde{\psi}^-(\mu, \theta) = -\frac{\xi}{b} \frac{\cosh \mu}{\cosh \mu_b} \sin \theta. \tag{3.8}$$

Since  $\tilde{U}$ ,  $\tilde{J}$ ,  $\nabla_{\varrho_{\text{eq}}}$  and  $\nabla J_{\text{eq}}$  all vanish inside the elliptical boundary, (3.6) is trivially satisfied. Note that in elliptical coordinates,  $\nabla^2 \chi = h^{-2}(\partial^2 \chi / \partial \mu^2 + \partial^2 \chi / \partial \theta^2)$ , where  $h = 1/|\nabla \mu| = 1/|\nabla \theta|$  is a scale factor, with  $h^2 = A^2(\cosh 2\mu + \cos 2\theta)/2$ .

When an ideal or resistive wall is present, the rigid-shift solutions (3.7) and (3.8) for the streamfunction and the perturbed flux in the plasma region retain their validity, while, in the vacuum region, the perturbed flux satisfies  $\nabla^2 \tilde{\psi}^+ = 0$ , whose solution can be best represented as

$$\tilde{\psi}^+(\mu, \theta) = -\frac{\xi_{\infty}}{b} \exp[-(\mu - \mu_b)] \sin \theta + \frac{\xi_{\text{ext}}}{b} \frac{\cosh \mu}{\cosh \mu_b} \sin \theta. \tag{3.9}$$

In this expression,  $\xi_{\infty}$  is the amplitude of the rigid vertical displacement in the limit where the wall is moved to infinity, and the term proportional to  $\xi_{\text{ext}}$  represents the contribution to the perturbed flux due to the image currents that form on the wall when this is at a finite distance from the plasma boundary. Continuity of flux at the plasma boundary requires that  $\xi = \xi_{\infty} - \xi_{\text{ext}}$ , and so the actual vertical displacement  $\xi$  is reduced, as compared with the



no-wall case, by the amount  $\xi_{\text{ext}}$ . A perturbed current sheet forms at the plasma boundary

$$\tilde{J}(\mu, \theta) = \tilde{j}_b(\theta)\delta(\mu - \mu_b) = \frac{1}{h^2} \left( \frac{\partial \tilde{\psi}^+}{\partial \mu} - \frac{\partial \tilde{\psi}^-}{\partial \mu} \right) \Bigg|_{\mu_b} \delta(\mu - \mu_b), \quad (3.10)$$

where  $\delta(x)$  is the Dirac delta function. A straightforward calculation yields the elliptical-angle modulation of the current sheet

$$\tilde{j}_b(\theta) = \frac{2(a + b)}{b^2(a^2 + b^2)} \frac{\xi_\infty \sin \theta}{1 + e_0 \cos 2\theta}. \quad (3.11)$$

Note that  $\tilde{j}_b(\theta)$  depends only on  $\xi_\infty$  and not on  $\xi_{\text{ext}}$ , as the current sheet at the plasma boundary does not depend on the wall image currents.

#### 4. Dispersion relation and quadratic forms

In this section, with the help of quadratic forms, we derive a dispersion relation for  $n = 0$  vertical modes, which depends on geometrical parameters,  $a$  and  $b$ , and on a function,  $D_w(\gamma)$ , determined by the geometry and the resistivity of the wall, which becomes independent of  $\gamma$  in the ideal wall limit.

Let us introduce the auxiliary streamfunction  $\tilde{\varphi}^\dagger$ , such that it equals the complex-conjugate streamfunction in the volume occupied by the plasma (up to  $\mu = \mu_b + \epsilon$ , i.e. including the perturbed current sheet at the plasma boundary), that we denote by the symbol  $\Omega$ , while  $\tilde{\varphi}^\dagger$  equals zero in the vacuum region. We multiply the perturbed plasma equation of motion (3.6) by  $\tilde{\varphi}^\dagger/2\gamma^*$  and integrate it over the whole volume extending to infinity. After standard manipulations, we obtain

$$-\gamma^2 \frac{1}{2} \int_\Omega d^3x \rho_{\text{eq}} \boldsymbol{\xi} \cdot \boldsymbol{\xi}^* = -\frac{1}{2} \int_\Omega d^3x \boldsymbol{\xi}^* \cdot \left[ (\tilde{\mathbf{J}} \times \mathbf{B}_{\text{eq}}) + (\mathbf{J}_{\text{eq}} \times \tilde{\mathbf{B}}) \right], \quad (4.1)$$

where  $\boldsymbol{\xi} = \mathbf{e}_z \times \nabla \tilde{\varphi} / \gamma$  is the displacement vector. Thus, the dispersion relation can be written as

$$-\gamma^2 = \delta W / \delta I, \quad (4.2)$$

where

$$\delta I = \frac{1}{2} \int_\Omega \rho_{\text{eq}} \boldsymbol{\xi} \cdot \boldsymbol{\xi}^* d^3x, \quad (4.3)$$

and

$$\delta W = -\frac{1}{2} \int_\Omega \boldsymbol{\xi}^* \cdot \mathbf{F}(\boldsymbol{\xi}) d^3x, \quad (4.4)$$

with  $\mathbf{F}(\boldsymbol{\xi}) = [(\tilde{\mathbf{J}} \times \mathbf{B}_{\text{eq}}) + (\mathbf{J}_{\text{eq}} \times \tilde{\mathbf{B}})]$  the force density operator in the limit where  $\beta$  effects are negligibly small. Note that, even though the potential energy integral is extended to the volume occupied by the plasma, wall effects are included in  $\delta W$  through the perturbed magnetic flux, which depends also on the contribution due to image currents that flow on the wall as the plasma boundary is displaced. As it will be shown in the following,  $\delta W$  is a real quantity, independent of the mode frequency, in the limit of an ideal wall, but it becomes frequency dependent when the wall is resistive.

Straightforward algebra, using  $d^3x = h^2 d\theta d\mu dz$ , leads to

$$\delta I = \frac{1}{2} \int_{\Omega} d^3x \rho_{\text{eq}} \frac{\nabla \tilde{\varphi} \cdot \nabla \tilde{\varphi}^*}{|\gamma|^2} = \frac{\pi}{2} ab L_z \xi^2, \tag{4.5}$$

where  $L_z$  is the length of the straight tokamak. Without loss of generality, we can take  $\xi$  to be real and to correspond to the amplitude of the vertical displacement introduced in the previous section. The perturbed energy integral is

$$\delta W = \frac{1}{2} \int_{\Omega} d^3x \left( \mathbf{e}_z \times \frac{\nabla \tilde{\varphi}^*}{\gamma^*} \right) \cdot (\tilde{J} \nabla \psi_{\text{eq}} + J_{\text{eq}} \nabla \tilde{\psi}). \tag{4.6}$$

The last term can be further manipulated, using the results for the perturbed streamfunction and the perturbed magnetic flux obtained in § 3.  $\delta W$  is written as the sum of two terms. The first term is

$$\begin{aligned} & \frac{1}{2} \int_{\Omega} d^3x \tilde{J} \nabla \psi_{\text{eq}} \cdot \left( \mathbf{e}_z \times \frac{\nabla \varphi^*}{\gamma^*} \right) \\ &= \frac{L_z}{2} \int_0^{2\pi} d\theta \int_0^{\mu_b + \epsilon} d\mu h^2 \tilde{j}_b(\theta) \delta(\mu - \mu_b) \nabla \psi_{\text{eq}} \cdot \left( \mathbf{e}_z \times \frac{\nabla \varphi^*}{\gamma^*} \right) = \frac{\pi}{2} \frac{a+b}{b^3} L_z \xi_{\infty} \xi. \end{aligned} \tag{4.7}$$

The second term can be expressed as

$$\begin{aligned} & \frac{1}{2} \int_{\Omega} d^3x J_{\text{eq}} \nabla \tilde{\psi} \cdot \left( \mathbf{e}_z \times \frac{\nabla \varphi^*}{\gamma^*} \right) \\ &= \frac{L_z}{2} \int_0^{2\pi} d\theta \int_0^{\mu_b + \epsilon} d\mu h^2 J_{\text{eq}} \nabla \tilde{\psi} \cdot \left( \mathbf{e}_z \times \frac{\nabla \varphi^*}{\gamma^*} \right) = -\frac{\pi}{2} \frac{a^2 + b^2}{ab^3} L_z \xi^2. \end{aligned} \tag{4.8}$$

It is convenient to introduce the quantity

$$D_w = \frac{\xi_{\text{ext}}}{\hat{e}_0 \xi_{\infty}}, \tag{4.9}$$

where  $\hat{e}_0 = e_0 b / (a + b)$ . Then, combining (4.7), (4.8) and (4.9), remembering that  $\xi = \xi_{\infty} - \xi_{\text{ext}}$ , we obtain

$$\delta W = -\frac{\pi}{2} L_z \frac{1 - a/b}{ab} \frac{1 - D_w}{1 - \hat{e}_0 D_w} \xi^2. \tag{4.10}$$

Thus, (4.2) yields the dispersion relation

$$\gamma^2 = \frac{1 - a/b}{a^2 b^2} \frac{1 - D_w}{1 - \hat{e}_0 D_w}. \tag{4.11}$$

This dispersion relation is ‘general’, in the sense that it can be applied to the three cases of interest, i.e. the no-wall limit, the ideal wall case and the resistive-wall case, as wall effects are included in (4.11) through the single stability function,  $D_w$ . In (4.11), parameters  $a$  and  $b$  are normalized to the scale length  $r_0$  defined below (3.2). Reintroducing dimensions, the dispersion relation (4.11) takes the form

$$(\gamma \tau_A)^2 = \frac{r_0^4}{a^2 b^2} \left( 1 - \frac{a}{b} \right) \frac{1 - D_w}{1 - \hat{e}_0 D_w}. \tag{4.12}$$

Thus, the mode’s stability depends on the quantity  $D_w$ , which is determined once the location of the wall and its nature, whether ideal or resistive, is decided. As shown in

§§ 4.1 and 4.2, if the wall is perfectly conducting,  $D_w$  is a real quantity, independent of  $\gamma$ , that reduces to the parameter  $D$  introduced in the heuristic model of S 2. In this case, the relevant dispersion relation is quadratic in  $\gamma$ , and the sign of  $\gamma^2$ , which depends on the sign of  $1 - D$ , determines the stability of vertical displacements in the ideal-MHD limit. However, if a resistive wall is considered, then  $D_w = D_w(\gamma)$  and the dispersion relation becomes cubic in  $\gamma$ , as discussed in § 4.3.

4.1. *Wall at infinity*

The first case we investigate is the no-wall limit, or equivalently, the case where the wall is moved to infinity. The analysis of § 3 shows that, in this case,  $\xi_{\text{ext}} = 0$ , hence  $D_w = 0$ . The vertical mode is unstable, with  $\gamma^2$  a positive real value (for  $b > a$ ), which reduces to zero in the circular limit,  $a = b$ . The mode growth rate is

$$\gamma = \frac{r_0^2}{ab} \left(1 - \frac{a}{b}\right)^{1/2} \tau_A^{-1} \equiv \gamma_\infty, \tag{4.13}$$

and  $\gamma^2$  can also be written in terms of the ellipticity parameter,

$$\gamma^2 = (1 - e_0)(1 + e_0 - \sqrt{1 - e_0^2})\tau_A^{-2} \equiv \gamma_\infty^2. \tag{4.14}$$

We remark that this result is valid for arbitrary values of  $e_0$  in the interval  $0 \leq e_0 \leq 1$ . In the limit of small ellipticity,  $\gamma_\infty$  reduces to  $\gamma_H$  in (2.3) and the mode growth rate agrees perfectly well with the heuristic result of § 2.

4.2. *Passive feedback stabilization: ideal wall*

Assume that the wall is represented by an elliptical coordinate surface,  $\mu = \mu_w$ , confocal to the elliptical plasma boundary at  $\mu = \mu_b$ , with  $\mu_w \geq \mu_b$ . If the wall is ideal, the perturbed flux in (3.9) must vanish at  $\mu = \mu_w$ , i.e.  $\tilde{\psi}^+(\mu_w, \theta) = 0$ . It follows that

$$\frac{\xi_{\text{ext}}}{\xi_\infty} = \frac{\exp(-(\mu_w - \mu_b)) \cosh \mu_b}{\cosh \mu_w} = \frac{1 + \exp(2\mu_b)}{1 + \exp(2\mu_w)}. \tag{4.15}$$

Now, let us use

$$a_w = A \sinh \mu_w, \quad b_w = A \cosh \mu_w, \tag{4.16a,b}$$

$$a = A \sinh \mu_b, \quad b = A \cosh \mu_b, \tag{4.17a,b}$$

where  $A = \sqrt{b_w^2 - a_w^2} = \sqrt{b^2 - a^2}$ , with  $b_w$  and  $a_w$  the major and minor semi-axes of the elliptical wall, respectively. It follows that

$$e^{2\mu_b} = \frac{b + a}{b - a}, \tag{4.18}$$

$$e^{2\mu_w} = \frac{b_w + a_w}{b_w - a_w}. \tag{4.19}$$

Using (4.15)–(4.19) and the definition of  $D_w$  in (4.9), we obtain

$$D_w = \frac{b^2 + a^2}{(b - a)^2} \frac{b_w - a_w}{b_w} \equiv D. \tag{4.20}$$

Note that, as the wall is moved further away from the plasma boundary, it becomes more and more ‘circular’, due to the assumption of confocality with the elliptical plasma

boundary. Therefore, as  $b_w/b \rightarrow \infty$ ,  $b_w \rightarrow a_w$  and  $D \rightarrow 0$ , as it should. We also observe that, apart from the extra term  $\hat{e}_0 D$  in the denominator of (4.11), the dispersion relation (4.11) with  $D_w = D$  agrees very well with the heuristic dispersion relation obtained in § 2. We can conclude that, if  $D > 1$ ,  $\gamma^2$  is negative, and thus the vertical mode oscillates with a real frequency

$$\omega = \pm \omega_0 = \pm \left[ \frac{D - 1}{1 - \hat{e}_0 D} \right]^{1/2} \gamma_\infty, \tag{4.21}$$

which reduces to  $\omega_H$  defined in (2.6) in the limit of small ellipticity. The dispersion relation is quadratic and the only solutions that can be extracted, in the limit  $D > 1$ , are the VDOM solutions. Thus, an ideal elliptical wall, confocal with the elliptical plasma boundary, can provide passive feedback stabilization of the vertical instability when  $D_w = D > 1$ .

The term  $\hat{e}_0 D$  can be neglected if it is small as compared with unity, but in fact it plays an important role if the wall coincides with the plasma boundary. Indeed,  $D$  reaches its maximum value in this limit, where  $\mu_w = \mu_b$ ,  $D = D_{\max} = (a + b)/(e_0 b) = 1/\hat{e}_0$  and the denominator in (4.21) vanishes. Therefore, in this special limit, the oscillation frequency goes to infinity, but also, the amplitude of the displacement,  $\xi = \xi_\infty - \xi_{\text{ext}}$ , goes to zero, as  $\xi_{\text{ext}} \rightarrow \xi_\infty$ . As a numerical example, take  $a_w = a$ ,  $b_w = b$  and  $b/a = 1.8$ . In this case,  $D_{\max} \approx 2.9$ . As the wall is placed further away from the plasma boundary, the value of  $D$  decreases monotonically, and a purely oscillatory solution is found for as long as  $D$  remains larger than unity.

It can be easily checked, using (4.15)–(4.19), that the marginally stable value,  $D = 1$ , is obtained when  $\mu_w = 2\mu_b$ , which corresponds to the elliptical wall intercepting the X-points. Thus, our model indicates that values of  $D < 1$ , for which no passive feedback stabilization is possible, are found when the X-points lie inside the volume bounded by the wall. We point out that this result is in perfect agreement with that obtained by Laval *et al.* (1974) on the basis of the ideal-MHD energy principle. However, this result holds true for the special case of confocal wall and plasma boundaries. For different wall shapes that fit more tightly with the plasma boundary, passive feedback stabilization due to the ideal wall does not necessarily require that the X-points lie beyond the wall. Furthermore, in real tokamak plasmas, additional coils and/or short-circuited plates located inside the vacuum chamber can contribute to passive feedback stabilization (Albanese *et al.* 2004; Portone 2017).

Finally, we point out that, as shown in Yolbarsop *et al.* (2021, 2022), if the plasma extends to the magnetic separatrix, as is normally the case for a divertor tokamak plasma, axisymmetric plasma currents associated with vertical displacement perturbations are driven in the vicinity of the magnetic X-points. As a consequence, these currents can also contribute to passive feedback stabilization of the vertical instability.

### 4.3. Passive feedback stabilization: resistive wall

Lastly, we consider the more realistic case of a resistive wall. In this situation the perturbed magnetic flux is not zero at the wall, but can diffuse across on the resistive-wall time scale. We identify three different regions: inside the elliptical boundary,  $\mu \leq \mu_b$ , where the perturbed flux  $\tilde{\psi}$  equals  $\tilde{\psi}^-$  given by (3.8); the vacuum region between the plasma boundary and the wall,  $\mu_b \leq \mu \leq \mu_w$ , where  $\tilde{\psi}$  equals  $\tilde{\psi}^+$  given by (3.9); and the vacuum outside the wall, where  $\tilde{\psi} = \tilde{\psi}_{\text{out}}$  is the solution of  $\nabla^2 \tilde{\psi}_{\text{out}} = 0$  that decays to zero at infinity. Focusing on vertical displacements with elliptical mode number  $m = 1$ , the relevant solution is

$$\tilde{\psi}_{\text{out}}(\mu, \theta) = \psi_0 \exp(-(\mu - \mu_w)) \sin \theta \quad \text{for } \mu \geq \mu_w + \delta_w, \tag{4.22}$$

where  $\delta_w$  is a small parameter representing the average width of the thin wall.

Two conditions at the wall determine the parameter  $\psi_0$  and  $D_w$ ; the latter will turn out to be a function of complex  $\gamma$ . The first condition is continuity of flux at the wall,  $\tilde{\psi}^+(\mu_w, \theta) = \tilde{\psi}_{\text{out}}(\mu_w, \theta)$ , which gives

$$\psi_0 = -\frac{\xi_\infty}{b} \exp(-(\mu_w - \mu_b)) + \frac{\xi_{\text{ext}} \cosh \mu_w}{b \cosh \mu_b}. \tag{4.23}$$

The second condition involves the current flowing along the wall. Consider the resistive Ohm’s law for the perturbed magnetic flux within the wall,  $\partial \psi_w / \partial t = (\eta c^2 / 4\pi) \nabla^2 \psi_w$ , where  $\eta$  is the wall resistivity. After proper normalization, we obtain

$$\nabla^2 \tilde{\psi}_w = \frac{\gamma}{\varepsilon_\eta} \tilde{\psi}_w, \tag{4.24}$$

where  $\varepsilon_\eta = (\eta \tau_A c^2) / (4\pi r_0^2)$  is the inverse of the relevant dimensionless Lundquist number. Since the wall is relatively thin, we can neglect the dependence on  $\mu$  of the perturbed flux at the right-hand side of (4.24). This approximation is similar to the standard constant- $\psi$  approximation used in magnetic reconnection theory. Set  $\tilde{\psi} = \hat{\psi}(\mu) \sin \theta$ . We assume the ordering  $\partial_\mu^2 \hat{\psi} \sim \hat{\psi} / \mu_w \delta_w \gg \hat{\psi}$ . Then, (4.24) can be approximated as

$$\frac{d^2 \hat{\psi}}{d\mu^2} = h^2 \frac{\gamma}{\varepsilon_\eta} \psi_0. \tag{4.25}$$

Integrating across the thin wall,

$$\int_{\mu_w}^{\mu_w + \delta_w} \frac{d^2 \hat{\psi}}{d\mu^2} d\mu = \int_{\mu_w}^{\mu_w + \delta_w} h^2 \frac{\gamma}{\varepsilon_\eta} \psi_0 d\mu. \tag{4.26}$$

The scale factor  $h$  is defined below (3.8). Strictly speaking,  $h$  depends on both  $\mu$  and  $\theta$ . However, in the limit of small wall ellipticity, which is assumed in the following, the  $\theta$  modulation of  $h$  along the wall is small, so that we can approximate  $h(\mu_w, \theta) \approx b_w$ . Carrying out the integration, we find

$$\left( \frac{d\hat{\psi}_{\text{out}}}{d\mu} - \frac{d\hat{\psi}^+}{d\mu} \right) \Big|_{\mu_w} = \frac{\gamma \delta_w b_w^2}{\varepsilon_\eta} \psi_0, \tag{4.27}$$

or equivalently

$$-\frac{\xi_\infty}{b} \exp(-(\mu_w - \mu_b)) - \frac{\xi_{\text{ext}} \sinh \mu_w}{b \cosh \mu_b} = \left( 1 + \frac{\gamma \delta_w b_w^2}{\varepsilon_\eta} \right) \psi_0. \tag{4.28}$$

Equations (4.23) and (4.28) are two equations that can be used to determine the two parameters,  $\psi_0 \propto \xi_\infty$ , and  $\xi_{\text{ext}} / \xi_\infty \propto D_w$ , cf. (4.9). After straightforward algebra, we obtain

$$D_w(\gamma) = D \frac{\gamma \tau_\eta}{1 + \gamma \tau_\eta}, \tag{4.29}$$

and

$$\psi_0 = -\frac{\xi_\infty}{b} \frac{b_w}{(a + b)} \frac{e_0 D}{(1 + \gamma \tau_\eta)}. \tag{4.30}$$

In these equations,  $D$  was defined in (4.15), and  $\tau_\eta = [b_w^3 / (a_w + b_w)] \delta_w / \varepsilon_\eta$  is the resistive-wall time (normalized to the relevant Alfvén time). Notice that the stability

parameter  $D_w$  depends on  $\gamma$  due to finite wall resistivity. In the ideal wall limit,  $\tau_\eta \rightarrow \infty$ ,  $D_w(\gamma) \rightarrow D$  reduces to the parameter  $D$  discussed in § 4.2. Also, (4.30) shows that the perturbed flux at the wall goes to zero in the ideal wall limit, as it should.

Substituting  $D_w(\gamma)$  in (4.11), one obtains the dispersion relation for vertical displacements in the case of feedback stabilization via a resistive wall

$$\gamma^3 + \gamma^2 \frac{1}{\tau_\eta} \frac{1}{1 - \hat{e}_0 D} + \gamma \omega_0^2 + \omega_0^2 \frac{1}{\tau_\eta} \frac{1}{1 - D} = 0, \quad (4.31)$$

with  $\omega_0$  defined in (4.21). It is reassuring that (4.31) agrees very well with the dispersion relation found heuristically in § 2, cf. (2.10). This is particularly true in the small ellipticity limit, where the term  $\hat{e}_0 D$  can be neglected and the frequency  $\omega_0$  reduces to  $\omega_H$ , cf. (2.6).

The three roots of this cubic dispersion relation are easily determined in the realistic limit  $\omega_0 \tau_\eta \gg 1$ . After straightforward algebra, for  $D > 1$ , one obtains two damped oscillatory roots and an unstable growing solution ( $\gamma = -i\omega$ )

$$\omega = \pm \omega_0 - i \frac{1}{2\tau_\eta} \frac{D(1 - \hat{e}_0)}{(D - 1)(1 - \hat{e}_0 D)}, \quad (4.32)$$

$$\gamma = \frac{1}{(D - 1)\tau_\eta}. \quad (4.33)$$

The two oscillatory, weakly damped roots of (4.32) correspond to the two VDOM that oscillate with a frequency slightly below the poloidal Alfvén frequency, as already found in § 4.2. The effect of a resistive wall is to introduce a small damping rate of the order of the inverse resistive-wall time. The third root, (4.33), corresponds to an unstable mode, growing on the resistive-wall time scale. Typical values of the resistive wall time in tokamak devices are of the order of a few milliseconds. As we have already pointed out in § 2, due to its slow growth, this non-rotating, unstable mode is normally suppressed by means of active feedback control systems (Albanese *et al.* 2004).

## 5. Conclusions

In this article, the dispersion relation for vertical plasma displacement normal modes has been derived analytically. Vertical displacements are axisymmetric modes of a toroidal tokamak plasma, with toroidal mode number  $n = 0$ . They cause an up–down motion of the entire plasma column, and as such are dominated by Fourier components with elliptical mode number  $m = 1$ . The up–down symmetry implies that the perturbed streamfunction is an even function of the elliptical angle  $\theta$  ( $\theta = 0$  corresponds to the horizontal direction), while the perturbed magnetic flux is an odd function of  $\theta$ . Our derivation is based on the reduced ideal-MHD model and on a simple, ‘straight-tokamak’ equilibrium, that assumes an elliptical plasma boundary and a uniform current density profile. This assumption is motivated by two considerations. Firstly, it is known that the stability and growth rate of vertical displacements depends on plasma shaping and on the total plasma current, but not on details of the current density profiles. Secondly, the assumed equilibrium is essentially the same as that used in the pioneering article by Laval *et al.* (1974). In that article, vertical stability was analysed based on the ideal-MHD energy principle. In our analysis, we carry out the complete normal mode analysis, which provides a solution for the mode structure and for the relevant dispersion relation, given by (4.12).

The method of quadratic forms, adopted in this article, together with the normal-mode solution for the mode structure, are shown to be an expedient way to obtain the relevant dispersion relation. The latter contains a parameter,  $D_w(\gamma)$ , which is a function of the

complex mode eigenvalue,  $\gamma = -i\omega$ , for the case of plasma confined by a resistive wall, see (4.29);  $D_w$  reduces to a constant  $D$  parameter in the limit of an ideal wall, see (4.20). Furthermore, when the wall is moved to infinity (the no-wall case),  $D \rightarrow 0$ . Consequently, the relevant dispersion relation is quadratic in  $\gamma$  for the case of an ideal wall (including the no-wall limit), while it is cubic in  $\gamma$  for the case of a resistive wall. Thus, an additional root (compared with the ideal wall limit) is found for the resistive-wall case. This root corresponds to a zero frequency, purely growing mode, with a growth time of the order of the resistive-wall time. Active feedback control systems applied to tokamak experiments concentrate on the suppression of this purely growing mode (Albanese *et al.* 2004).

The other two roots, that we have dubbed VDOM, are purely oscillatory for the case of an ideal wall, provided the parameter  $D$  is larger than unity, which sets a condition on the distance of the ideal wall from the plasma. These oscillatory modes are actually weakly damped by wall resistivity, see (4.32). Therefore, if their oscillation frequency is sufficiently well separated from the bandwidth of the vertical stabilization closed loop, these modes do not have a significant impact on the active feedback control systems. Nevertheless, we would like to bring the attention of the tokamak physics community on the importance of these oscillatory solutions. As we have shown in this article (see also Porcelli *et al.* 2021; Barberis *et al.* 2022), their oscillation frequency is slightly below the poloidal Alfvén frequency, which makes these modes immune to Alfvén continuum damping. Thus, these modes are only weakly damped by wall resistivity. On the other hand, they can interact resonantly with fast ion populations, which are present in a tokamak plasma due to auxiliary heating and/or as fusion reaction products. Under special circumstances, discussed in some detail in Barberis *et al.* (2022), this resonant interaction may drive the VDOM unstable.

Indeed, the theory presented in this article is motivated in part by the observation of saturated  $n = 0$  fluctuations, with a frequency of the order of the poloidal Alfvén frequency, in recent JET experiments where fast ions are produced by auxiliary heating (Oliver *et al.* 2017; Kiptily *et al.* 2021). In those articles, the observations were tentatively interpreted in terms of a saturated  $n = 0$  global Alfvén eigenmode (GAE) (Villard & Vaclavik 1997). It is early for us to conclude whether, in fact, the mode observed at JET is a VDOM driven unstable by the fast ion resonance, rather than a GAE: more experiments are required, but also, the theory presented here ought to be developed further. Nevertheless, we can indicate the main points of distinction between GAE and VDOM that may facilitate the experimental identification. These are basically three. First, the GAE mode frequency for  $n = 0$  is given by (Villard & Vaclavik 1997)  $\omega_{\text{GAE}} = v_A/qR = \tau_A^{-1}$ , where  $\tau_A$  is the poloidal Alfvén time as defined below (2.3) of this article. On the other hand, the VDOM mode frequency is given by (4.32), and, taking the parameter  $D$  above unity, but anyway of order unity, it falls below the GAE mode frequency, since the ellipticity parameter  $e_0$  is typically small. Secondly, the VDOM frequency scales as the square root of  $e_0$ , while the  $n = 0$  GAE mode frequency is independent of elongation. Indeed, the GAE would survive in the circular limit, while the VDOM would not. Thirdly, and perhaps most importantly, the VDOM mode structure is different from that of the GAE. The VDOM is a vertical mode, corresponding to a vertical oscillation of the plasma cross-section, with the relevant perturbed flux an odd function of the poloidal angle. This signature would be easily detected by magnetic perturbation coils placed on top and bottom of the plasma column. The GAE mode structure favours instead a ballooning type of parity, with the perturbed flux being an even function of the poloidal angle.

A numerical estimate of the VDOM frequency for realistic JET parameters can be provided as follows. Let us consider the JET discharges discussed in Oliver *et al.* (2017), where saturated  $n = 0$  oscillations driven unstable by fast ions were observed. For these

discharges, the main plasma species was deuterium, ion density  $n_i \approx 4.0 \times 10^{19} \text{ m}^{-3}$  and  $B'_p \approx 1.0 \text{ T m}^{-1}$ , yielding a poloidal Alfvén time  $\tau_A \approx 0.4 \text{ } \mu\text{s}$ . The elongation parameter was  $\kappa = b/a \approx 1.3$ , corresponding to ellipticity  $e_0 \approx 0.26$  and to the no-wall growth rate  $\gamma_\infty \approx 1.2 \times 10^6 \text{ s}^{-1}$ . In order to estimate the parameter  $D$  appearing in (4.21), let us take  $a_w/a = 1.2$  and  $b_w/b = 1.1$  (since, for confocal ellipses,  $b_w^2 - a_w^2 = b^2 - a^2$ ). Then,  $D \approx 5.2$ ,  $\hat{e}_0 D \approx 0.77$  and  $\omega_0 \approx 4\gamma_\infty \approx 5 \times 10^6 \text{ s}^{-1}$ , or  $\omega_0 \approx 800 \text{ kHz}$ , which is within a factor of two of the observed frequency of saturated  $n = 0$  modes in the mentioned JET experiment. However, JET plasmas are bounded by the divertor separatrix and a more appropriate estimate of the theoretical mode frequency should take into account X-point effects, as argued in Yolbarsop *et al.* (2021). Clearly, an accurate determination of the theoretical VDOM frequency also requires more realistic equilibrium profiles and numerical work.

It is reassuring to see that the dispersion relation derived in this article, (4.12), agrees fairly well with the heuristic result of § 2, see (2.9), in the limit where the  $\hat{e}_0 D$  appearing in the expression for  $\omega_0$  is small.

Finally, the case where a magnetic divertor separatrix limits the plasma was not discussed in this article, but was treated in some detail in Yolbarsop *et al.* (2021, 2022). The main result of that work is that, even for the no-wall case, axisymmetric current sheets localized in the vicinity of the magnetic X-point(s) on the divertor separatrix, induced by vertical displacement perturbations, lead to passive feedback stabilization. The reason is that X-points are resonant points for ideal-MHD perturbations with toroidal mode number  $n = 0$ . As a result, flux pile-up will occur in the presence of ideal-MHD flows having the appropriate symmetry around the resonant points, and this is indeed the symmetry of interest for vertical displacements. Flux pile-up is the reason for the occurrence of current sheets, which have the appropriate sign and magnitude to ‘push back’ the plasma drifting vertically towards a magnetic X-point. In this sense, these X-point currents have the same effect on the plasma as that of currents induced by vertical displacements on an ideal (or nearly ideal) wall. It remains to be seen what will happen to the zero-frequency unstable root resonating on magnetic X-points when the effect of finite plasma resistivity is taken into account.

## Acknowledgements

The authors acknowledge useful discussions with F. Villone (University of Naples ‘Federico II’) on methods used for active feedback control of the vertical instability. The authors would also like to thank the authors of Oliver *et al.* (2017), J. Oliver, B. Breizman and S. Sharapov, for useful discussions on numerical simulations and the interpretation of saturated  $n = 0$  oscillations observed at JET.

*Editor Peter Catto thanks the referees for their advice in evaluating this article.*

## Funding

This work was partially supported by the National Natural Science Foundation of China under Grant No. 11775220 and the National Magnetic Confinement Fusion Energy Development Program of China under Grant No. 2017YFE0301702. This work has been carried out within the framework of the EUROfusion Consortium and has received funding from the Euratom Research and Training Programme (Grant Agreement No 101052200 EUROfusion). Views and opinions expressed are, however, those of the authors only and do not necessarily reflect those of the European Union or the European Commission.



Neither the European Union nor the European Commission can be held responsible for them.

### Declaration of interests

The authors report no conflict of interest.

### REFERENCES

- ALBANESE, R., MATTEI, M. & VILLONE, F. 2004 Prediction of the growth rates of VDEs in JET. *Nucl. Fusion* **44**, 999.
- BARBERIS, T., PORCELLI, F. & YOLBARSOP, A. 2022 Fast-ion-driven vertical modes in magnetically confined toroidal plasmas. *Nucl. Fusion* **62**, 064002.
- CLAUSER, C.F., JARDIN, S.C. & FERRARO, N.M. 2019 Vertical forces during vertical displacement events in an ITER plasma and the role of halo currents. *Nucl. Fusion* **59**, 126037.
- FITZPATRICK, R. 2009 A simple ideal magnetohydrodynamical model of vertical disruption events in tokamaks. *Phys. Plasmas* **16** (1), 012506.
- GRANETZ, R.S., HUTCHINSON, I.H., SORCI, J., IRBY, J.H., LABOMBARD, B. & GWINN, D. 1996 Disruptions and halo currents in Alcator C-Mod. *Nucl. Fusion* **36** (5), 545–556.
- HAAS, E.A. 1975 Stability of a high- $\beta$  tokamak to uniform vertical displacements. *Nucl. Fusion* **15**, 407.
- KIPTILY, V.G., FITZGERALD, M., KAZAKOV, YE.O., ONGENA, J., NOCENTE, M., SHARAPOV, S.E., DREVAL, M., ŠTANCAR, Z., CRACIUNESCU, T., GARCIA, J., *et al.* 2021 Evidence for Alfvén eigenmodes driven by alpha particles in D-<sup>3</sup>He fusion experiments on JET. *Nucl. Fusion* **61** (11), 114006.
- KREBS, I., ARTOLA, F.J., SOVINEC, C.R., JARDIN, S.C., BUNKERS, K.J., HOELZL, M. & FERRARO, N.M. 2020 Axisymmetric simulations of vertical displacement events in tokamaks: A benchmark of M3D-C<sup>1</sup>, NIMROD, and JOREK. *Phys. Plasmas* **27**, 022505.
- LAVAL, G., PELLAT, R. & SOULE, J.L. 1974 Hydromagnetic stability of a current-carrying pinch with noncircular cross section. *Phys. Fluids* **17**, 835.
- LAZARUS, E.A., LISTER, J.B. & NEILSON, G.H. 1990 Control of the vertical instability in tokamaks. *Nucl. Fusion* **30**, 111.
- LISTER, J.B., LAZARUS, E.A., KELLMAN, A.G., MORET, J.-M., FERRON, J.R., HELTON, F.J., LAO, L.L., LEUER, J.A., STRAIT, E.J., TAYLOR, T.S., *et al.* 1990 Experimental study of the vertical stability of high decay index plasmas in the DIII-D tokamak. *Nucl. Fusion* **30** (11), 2349.
- OKABAYASHI, M. & SHEFFIELD, G. 1974 Vertical stability of elongated tokamaks. *Nucl. Fusion* **14** (2), 263–265.
- OLIVER, H.J.C., SHARAPOV, S.E., BREIZMAN, B.N. & ZHENG, L.-J. 2017 Axisymmetric global Alfvén eigenmodes within the ellipticity-induced frequency gap in the Joint European Torus. *Phys. Plasmas* **24** (12), 122505.
- OLOFSSON, K.E.J. 2022 Fast calculation of the tokamak vertical instability. *Plasma Phys. Control. Fusion* **64**, 072001.
- PERRONE, M. & WESSON, J. 1981 Stability of axisymmetric modes in JET. *Nucl. Fusion* **21**, 871.
- PFEFFERLÉ, D. & BHATTACHARJEE, A. 2018 Algebraic motion of vertically displacing plasmas. *Phys. Plasmas* **25**, 022516.
- PORCELLI, F. & YOLBARSOP, A. 2019 Analytic equilibrium of “straight tokamak” plasma bounded by a magnetic separatrix. *Phys. Plasmas* **26**, 054501.
- PORCELLI, F., YOLBARSOP, A., BARBERIS, T. & FITZPATRICK, R. 2021 Resonant axisymmetric modes. *J. Phys.: Conf. Ser.* **1785** (1), 012004.
- PORTONE, A. 2017 Active and passive stabilization of  $n = 0$  RWMs in future tokamak devices. *Nucl. Fusion* **57**, 126060.
- REBHAN, E. 1975 Stability boundaries of tokamaks with respect to rigid displacements. *Nucl. Fusion* **15**, 277.
- RICCARDO, V. & JET EFDA CONTRIBUTORS 2009 Progress in understanding halo current at jet. *Nucl. Fusion* **49**, 055012.

- STRAIT, E.J., LAO, L.L., LUXON, J.L. & REIS, E.E. 1991 Observation of poloidal current flow to the vacuum vessel wall during vertical instabilities in the DIII-D tokamak. *Nucl. Fusion* **31** (3), 527–534.
- STRAUSS, H.R. 1976 Nonlinear, three-dimensional magnetohydrodynamics of noncircular tokamaks. *Phys. Fluids* **19**, 134.
- VILLARD, L. & VACLAVIK, J. 1997 Alfvén frequency modes and global Alfvén eigenmodes. *Nucl. Fusion* **37** (11), 351.
- WAGNER, F., BECKER, G., BEHRINGER, K., CAMPBELL, D., EBERHAGEN, A., ENGELHARDT, W., FUSSMANN, G., GEHRE, O., GERNHARDT, J., GIERKE, G.V., *et al.* 1982 Regime of improved confinement and high beta in neutral-beam-heated divertor discharges of the ASDEX tokamak. *Phys. Rev. Lett.* **49** (19), 1408.
- YOLBARSOP, A., PORCELLI, F. & FITZPATRICK, R. 2021 Impact of magnetic X-points on the vertical stability of tokamak plasmas. *Nucl. Fusion* **61** (11), 114003.
- YOLBARSOP, A., PORCELLI, F., LIU, W. & FITZPATRICK, R. 2022 Analytic theory of ideal-MHD vertical displacements in tokamak plasmas. *Plasma Phys. Control. Fusion* **64**, 105002.
- ZAKHAROV, L.E., GALKIN, S.A., GERASIMOV, S.N. & CONTRIBUTORS JET-EFDA 2012 Understanding disruptions in tokamaks. *Phys. Plasmas* **19** (5), 055703.